Electronic Supplementary Material (ESI) for Dalton Transactions.

Electronic Supporting Information

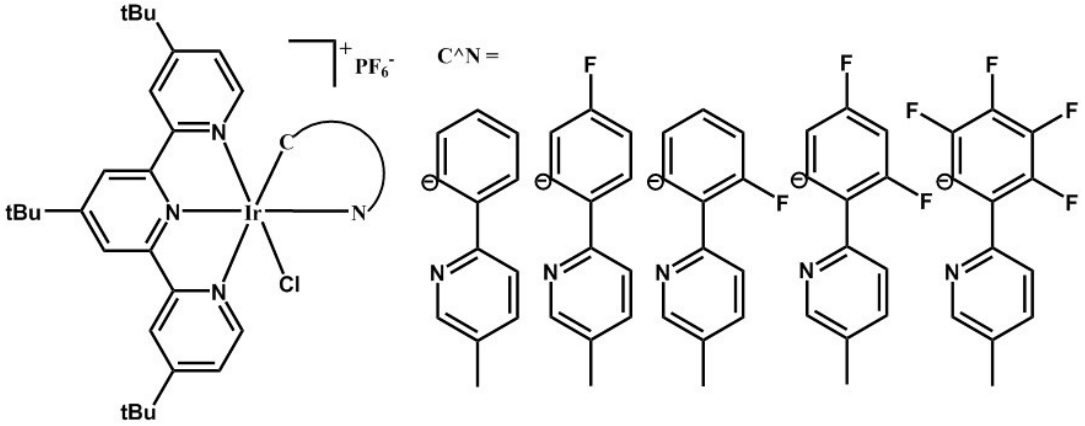

Scheme S1

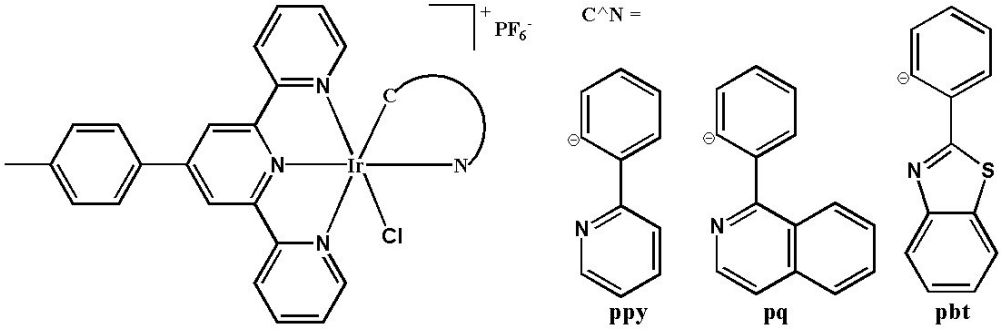

Scheme S2

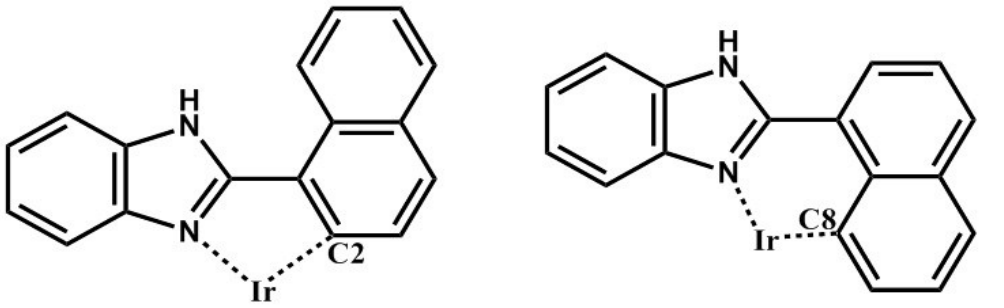

five-membered ring chelating mode **six-membered ring chelating mode**

Scheme S3

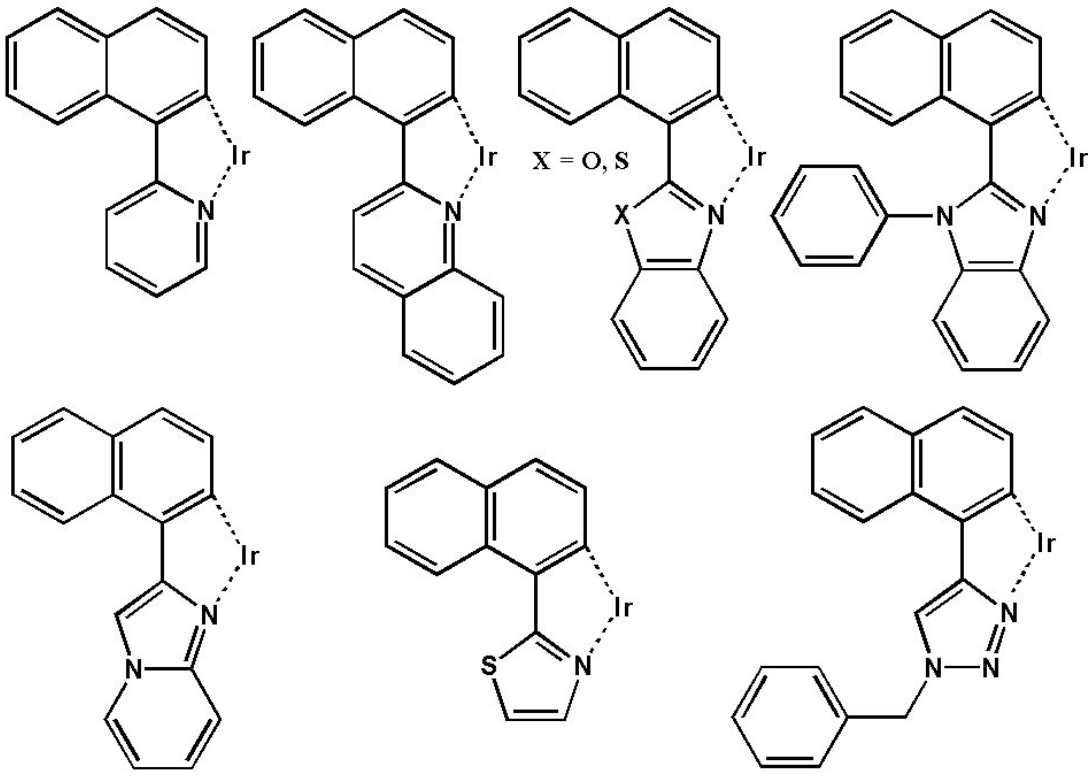

Scheme S4

Materials and Physical Measurements

Compound [Ir(tpy)Cl_3] (tpy = 2,2':6',2''-terpyridine) was prepared according to the literature.[S1] All other reagents were commercially available and used without further purification. Elemental analyses were performed on a Perkin Elmer 240C elemental analyzer. IR spectra were obtained as KBr disks on a VECTOR 22 spectrometer. ^{1}H NMR spectra were recorded at room temperature with a 400 MHz BRUKER spectrometer. Powder XRD patterns were recorded on a BRUKER D8 ADVANCE X-ray diffractometer. UV-vis absorption spectra were measured on a Cary 100 spectrophotometer. Luminescence spectra were measured using a Hitachi F-4600 fluorescence spectrometer. The luminescence lifetimes were measured at room temperature on a HORIBA FL-3 Spectrofluorometer with a 370 nm LED pulsed from a NanoLED resource. The photoluminescence quantum yields of **Ir-O** and **Ir-R** were measured by a relative method by comparison with a standard, a solution of quinine sulfate in 0.5 M H_2SO_4 (Φ = 54.6%, λ_{ex} = 366 nm).[S2]

1. Synthesis of 2-naphthalen-1-yl-1 *H*-benzoimidazole (nbiH)

A mixture of 1-naphthaldehyde (2 mmol, 312 mg), 1,2-diaminobenzene (2 mmol, 216 mg), $MgCl_2 \cdot 6H_2O$ (0.2 mmol, 40.6 mg) and DMF (10 mL) in an open flask was stirred at 80 ^oC for 10 hours. The reaction was mixed with CH_3COOCH_3 (40 mL). This mixture was washed with saturated NaCl aqueous solution (25 mL*5). The CH_3COOCH_3 solution was dried with $MgSO_4$, filtered, and then evaporated. The residue was purified through silica column chromatography using ethyl acetate–petroleum ether (v/v = 10-20/100) solution, obtaining a white solid with a yield of 400 mg (82% based on 1-naphthaldehyde). Anal. found (calcd) for $C_{17}H_{12}N_2$: C, 83.64 (83.58); H, 5.13 (4.95), N, 11.65 (11.47). IR (KBr, cm^{-1}): 3047(w), 2957(w), 2858(w), 2752(w), 2656(w), 1591(w), 1533(w), 1506(w), 1448(s), 1402(s), 1362(m), 1333(w), 1281(m), 1230(w), 1140(w), 1074(w), 1038(w), 1016(w), 951(w), 805(s), 774(s), 748(s), 445(w). ^1H NMR (400 MHz, DMSO-d_6), δ (ppm): 7.26 (broad, 2H from the benzene ring of benzene-imidazole moiety), 7.57-7.71 (m, 4H), 7.77 (d, J = 8Hz, 1H) [7.57-7.79 ppm: total 5H from naphthalene ring], 8.01-8.06 (m, 2H from the benzene ring of benzene-imidazole moiety), 8.09 (d, J = 8 Hz, 1H), 9.10 (d, J = 8 Hz, 1H) [8.09-9.10 ppm: total 2H from naphthalene ring].

2. Syntheses of Ir-O and Ir-R with molecular formula [Ir(tpy)(nbi)Cl](PF$_6$)

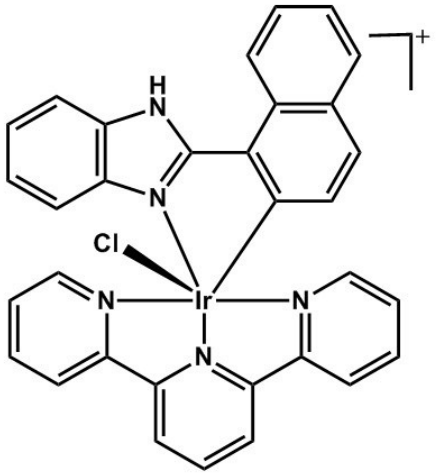

Ir-O cation

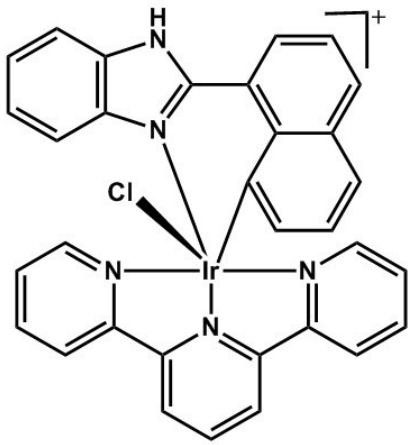

Ir-R cation

A mixture of $Ir(tpy)Cl_3$ (0.17 mmol, 91 mg), nbiH (0.34 mmol, 85 mg) in

ethylene glycol (25 mL) was heated in an oil bath (190 °C) under argon for one day. After adding saturated KPF_6 aqueous solution (20 mL), the resultant residue was filtered, and then purified through silica column chromatography using CH_3OH-CH_2Cl_2 (v/v = 0-3/100) solution, obtaining a yellow solid of **Ir-O** with a yield of 34 mg [24% based on Ir(tpy)Cl_3] and a red solid of **Ir-R** with a yield of 62 mg [43% based on Ir(tpy)Cl_3].

It should be noted that we also carried out this reaction at 135 °C, obtaining the yellow solid of **Ir-O** with a yield of 27 mg [19% based on Ir(tpy)Cl_3] and the red solid of **Ir-R** with a yield of 68 mg [47% based on Ir(tpy)Cl_3].

For complex **Ir-O**: Anal. found (calcd) for $C_{32}H_{22}N_5F_6PClIr$: C, 45.35 (45.26); H, 2.89 (2.61), N, 8.34 (8.25). IR (KBr, cm^{-1}): 3423(w), 2924(w), 1606(w), 1577(w), 1528(w), 1455(m), 1397(w), 1337(w), 1249(w), 848(s), 773(m), 558(w), 440(w). ^1H NMR (400 MHz, DMSO-d_6), δ (ppm): 6.23 (d, J = 8 Hz, 1H), 7.32 (d, J = 8 Hz, 1H), 7.42-7.48 (m, 4H), 7.54 (t, 1H), 7.72 (t, 1H) [6.23-7.72 ppm: total 8H from nbiH ligand], 7.77-7.79 (m, 3H, 2H from nbiH ligand and 1H from tpy ligand), 7.93 (d, J = 8 Hz, 1H), 8.17 (2t, 2H), 8.59 (t, 1H), 8.71-8.78 (m, 3H), 8.96 and 8.98 (2d, 2H), 9.04 (d, J = 8 Hz, 1H) [7.93-9.06 ppm: total 10H from typ ligand].

For complex **Ir-R**: Anal. found (calcd) for $C_{32}H_{22}N_5F_6PClIr$: C, 45.38 (45.26); H, 2.83 (2.61), N, 8.30 (8.25). IR (KBr, cm^{-1}): 3406(w), 3097(w), 3042(w), 1605(w), 1560(w), 1527(w), 1453(w), 1433(w), 1417(w), 1398(w), 1343(w), 1249(w), 1157(w), 1085(w), 973(w), 8520(s), 770(s), 558(w), 450(w). ^1H NMR (400 MHz, DMSO-d_6), δ (ppm): 6.10 (d, J = 8 Hz, 1H), 6.77 (t, 1H), 7.26-7.34 (m, 2H), 7.46-7.52 (m, 3H), 7.66 (t, 1H), 7.79 (d, J = 8 Hz,1H,), 7.90 (d, J = 8 Hz, 1H) [6.10-7.90 ppm: total 10H from nbiH ligand], 8.16 (2t, 2H), 8.33 and 8.35 (2d, 2H), 8.45-8.50 (m, 2H), 8.69-8.72 (m, 3H), 8.82 and 8.84 (d, 2H) [8.15-8.84 ppm: total 11H from typ ligand].

The orange plate crystals of **Ir-O**·Et_2O·CH_3COCH_3 were grown from slow diffusion of diethyl ether vapor into a solution of **Ir-O** in acetone. Its powder XRD pattern shows broad peaks due to fast loss of solvent molecules (Et_2O and CH_3COCH_3). Thus we have not given a comparison between experimental and simulated XRD patterns of **Ir-O**·Et_2O·CH_3COCH_3. The red needlelike single crystal

of **Ir-R** was obtained as a monophasic material based on the powder XRD pattern, through the evaporation of its solution of $CHCl_3$ and CH_3OH.

X-Ray crystallographic studies

Single crystal of dimensions 0.20 × 0.05 × 0.02 mm^3 for **Ir-O**·Et_2O·CH_3COCH_3 was used for structural determination on a Rigaku FRE+ CCD diffractometer equipped with VHF Varimax confocal mirrors and an AFC10 goniometer and HG Saturn 724+ detector using graphite-monochromated Mo Kα radiation (λ = 0.710 73 Å) at 100(2) K. Single crystal of dimensions 0.24 × 0.15 × 0.12 mm^3 for **Ir-R** was used for structural determination on a Bruker SMART APEX CCD diffractometer using graphite-monochromated Mo Kα radiation (λ = 0.710 73 Å) at room temperature. A hemisphere of data was collected in the θ range 1.82 to 25.03° for **Ir-O**·Et_2O·CH_3COCH_3 and 1.53 to 25.00° for **Ir-R** using a narrow-frame method with scan widths of 0.30° in ω and an exposure time of 10 s per frame. Numbers of observed and unique reflections are 41775 and 7263 (R_{int} = 0.0702) for **Ir-O**·Et_2O·CH_3COCH_3, and 32375 and 5335 (R_{int} = 0.0530) for **Ir-R**, respectively. The data were integrated using the Siemens *SAINT* program,[S3] with the intensities corrected for Lorentz factor, polarization, air absorption, and absorption due to variation in the path length through the detector faceplate. Multi-scan absorption corrections were applied. The structures were solved by direct methods and refined on F^2 by full matrix least squares using *SHELXTL*.[S4] All the non-hydrogen atoms were located from the Fourier maps, and were refined anisotropically. All H atoms were refined isotropically, with the isotropic vibration parameters related to the non-H atom to which they are bonded. It should be noted that the single crystals of complex **Ir-O**·Et_2O·CH_3COCH_3 is extremely thin orange plates, thus the present crystal data of this complex shows high R_1 value (R_1 = 0.0928 [$I>2\sigma(I)$]). In the structural refinement of **Ir-O**·Et_2O·CH_3COCH_3, SQUEEZE was used to removed a highly disordered region (possible some Et_2O and acetone molecules). Additionally, ISOR, DFIX were used to obtain a better refinement results. The crystallographic data for compounds **Ir-O**·Et_2O·CH_3COCH_3 and **Ir-R** are listed in Table S2, and selected bond lengths and

angles are given in Tables S3 and S4. CCDC 1570575 and 1570576 contain the supplementary crystallographic data of **Ir-O**·Et_2O·CH_3COCH_3 and **Ir-R**, which can be obtained free of charge from the Cambridge Crystallographic Data Centre via www.ccdc.cam.ac.uk/data_request/cif.

Cell culture and MTT assays

HeLa cells were cultured in high-glucose Dulbecco's Modified Eagle Medium (DMEM) supplemented with 10% fetal bovine serum and 1% penicillin/streptomycin at 37 °C in CO_2 incubator (95% relative humidity, 5% CO_2). Cytotoxicity of complexes **Ir-O** and **Ir-R** against HeLa cells was measured using methyl thiazolyl tetrazolium (MTT) assay. Briefly, approximately 5000 cells were seeded in a 96-well plate. After cell adherence overnight, the medium was removed, and the cells were washed twice with phosphate-buffered saline (PBS). Then a series of different concentrations of **Ir-O** / **Ir-R** (10, 20, 40, 60, or 100 μM) in 100 μL of FBS-free DMEM medium were added and incubated for 24 h. This was followed by the addition of 50 μL of 1× MTT reagent to each well and the plate was kept at 37 °C for 4 h. Then the medium was carefully removed, and 100 μL of DMSO was added to each well followed by shaking for 10 min. The % viability was calculated as a ratio of absorbance at 490 nm measured by a Spark™ Multimode Microplate Reader (Tecan Austria GesmbH).

Cellular imaging and colocalization assay

HeLa cells (~5 × 10^4) were plated onto glass-bottom dish (In Vitro Scientific, D35-20-1-N) and allowed to grow overnight. The culture medium was removed and washed with PBS, Following incubation with **Ir-O** or **Ir-R** at 20 μM in FBS-free DMEM at 37 °C for 1 h, 3 h and 6 h. After that, the medium was removed, and the cells were washed with PBS three times. Fluorescence imaging was performed under a Leica TCS SP5 confocal laser scanning microscope. For **Ir-O**, the excitation was 405 nm, and the emission was collected from 555−615 nm wavelength. For **Ir-R**, the excitation was 405 nm, and the emission was collected from 585−645 nm wavelength.

For colocalization studies, HeLa cells were incubated with **Ir-O** (20 μM) for 3 hous. Then the cells were washed with PBS three times, and lysosomes were further stained with 1 μM Lyso-tracker Green DND-26 at 37 °C for 15 min. After that, the medium was removed, and the cells were washed with PBS three times. Luminescence imaging was performed under a Leica TCS SP5 confocal laser scanning microscope. Emission from **Ir-O** was collected from 555−615 nm wavelength with the excitation at 405 nm, and emission from Lyso-tracker Green DND-26 was collected at green channel from 530 to 580 nm with excitation at 514 nm.

Table S1 Electrospray mass spectrometry (ES-MS) data of **Ir-O** and **Ir-R**

Compound	**Ir-O**	**Ir-R**
(ES-MS) data	704.25 from $[Ir(tpy)(nbi)Cl]^+$	704.42 from $[Ir(tpy)(nbi)Cl]^+$

Table S2 Crystallographic data of **Ir-O**·Et_2O·CH_3COCH_3 and **Ir-R**

	Ir-O·Et_2O·CH_3COCH_3	**Ir-R**
Formula	$C_{39}H_{38}N_5O_2F_6PClIr$	$C_{32}H_{22}N_5F_6PClIr$
M	981.36	849.16
Crystal system	Monoclinic	Orthorhombic
Space group	$P2_1/c$	*Pccn*
T/K	100(2)	296(2)
a/Å	15.5188(7)	22.8432(12)
b/Å	8.5784(3)	16.3316(9)
c/Å	30.9458(13)	16.2218(9)
β / °	92.578(4)	
V/Å^3	4115.5(3)	6051.8(6)
Z	4	8
D_c (g cm^{-3})	1.584	1.864
F(000)	1944	3296
GooF on F^2	1.263	1.033
,	0.0928, 0.2143	0.0304, 0.0762
R_1, wR_2 (all data)[a]	0.1167, 0.2249	0.0494, 0.0828
$(\Delta\rho)_{max}$,$(\Delta\rho)_{min}$/e Å^{-3}	4.612， -3.573	1.196, -0.882

[a] $R_1 = \Sigma||F_o|-|F_c||/\Sigma|F_o|$; $wR_2=[\Sigma w(F_o^2-F_c^2)^2/\Sigma w(F_o^2)^2]^{1/2}$

Table S3 Selected bond lengths (Å) and angles (°) for **Ir-O**·Et_2O·CH_3COCH_3

Ir1-N1	2.052(13)	Ir1-C2	2.065(16)
Ir1-N3	2.055(13)	Ir1-C11	2.447(4)
Ir1-N4	1.959(12)	N1-C11	1.360(19)
Ir1-N5	2.047(12)	N2-C11	1.34(2)
N4-Ir1-N5	81.0 (5)	N1-Ir1-C2	79.4(6)
N4-Ir1-N1	174.0(5)	N3-Ir1-C2	89.9(5)
N5-Ir1-N1	99.0(5)	N4-Ir1-Cl1	87.1(4)
N4-Ir1-N3	80.0(5)	N5-Ir1-Cl1	86.7(4)
N5-Ir1-N3	161.0(5)	N1-Ir1-Cl1	98.9(4)
N1-Ir1-N3	99.8(5)	N3-Ir1-Cl1	92.7(4)
N4-Ir1-C2	94.6(6)	C2-Ir1-Cl1	177.1(4)
N5-I1-C2	91.2(5)		

Table S4 Selected bond lengths (Å) and angles (°) for **Ir-R**

Ir1-N1	2.063(4)	Ir1-C8	2.058(5)
Ir1-N3	2.054(4)	Ir1-Cl1	2.4638(13)
Ir1-N4	1.960(4)	N1-C11	1.346(6)
Ir1-N5	2.050(4)	N2-C11	1.348(7)
N4-Ir1-N5	80.70(17)	N3-Ir1-N1	100.60(15)
N4-Ir1-N3	80.22(17)	C8-Ir1-N1	88.44(17)
N5-Ir1-N3	160.87(16)	N4-Ir1-Cl1	87.68(12)
N4-Ir1-C8	89.81(17)	N5-Ir1-Cl1	87.04(12)
N5-Ir1-C8	86.15(18)	N3-Ir1-Cl1	90.83(12)
N3-Ir1-C8	95.14(18)	C8-Ir1-Cl1	173.04(15)
N4-Ir1-N1	178.13(16)	N1-Ir1-Cl1	93.98(11)
N5-Ir1-N1	98.52(15)		

Table S5 Photophysical properties of **Ir-O**, **Ir-R**, nbiH and tpy [DMSO-PBS (v/v=1/9), C_2H_5OH-CH_3OH (v/v = 3/1)].

Compound	Medium	λ_{abs} (nm)	λ_{em} (nm)	Lifetime (ns)	quantum yield
Ir-O	CH_3CN (298 K)	269, 314, 325, 384, and a tail to 570	581	165 (93%), 296 (7%)	2.1%
	DMSO-PBS (298 K)	282, 313, 325, 377, and a tail to 570	580	-	0.35%
	EtOH-MeOH (77 K)	-	552, 599 and 655	-	-
Ir-R	CH_3CN (298 K)	280, 316, 376, and a tail to 570	612	86 (91%), 169 (9%)	0.56%
	DMSO-PBS (298 K)	287, 316, 375, and a tail to 570	610	-	0.20%
	EtOH-MeOH (77 K)	-	581 and 633	-	-
nbiH	CH_3CN (298 K)	312	-	-	-
tpy	CH_3CN (298 K)	279	-	-	-

Table S6 Oil-water partition coefficient of **Ir-O** and **Ir-R**.

Compound	**Ir-O**	**Ir-R**
ε / $M^{-1}cm^{-1}$	24930	24440
$[solute]_{o,e}$/μM	107.293	44.775
$[solute]_{w,e}$/μM	178.062	233.365
log P	-0.220	-0.717

Fig. S1 The photographs of **Ir-O** (left) and **Ir-R** (right) under room light.

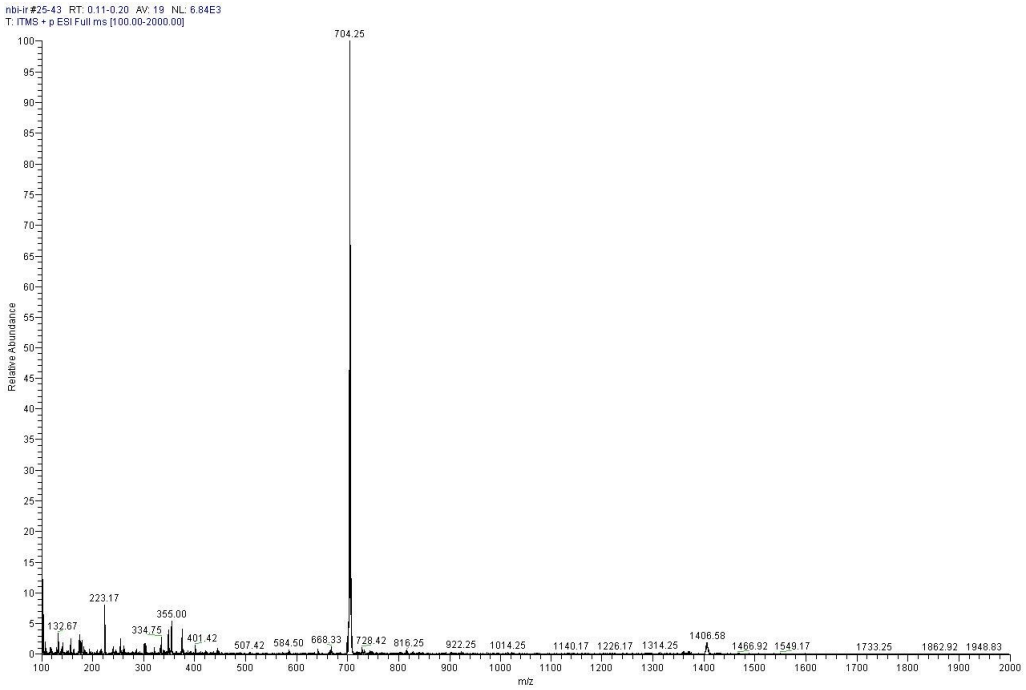

Fig. S2 Electrospray mass spectrometry (ES-MS) of **Ir-O** in CH_2Cl_2-CH_3OH solution.

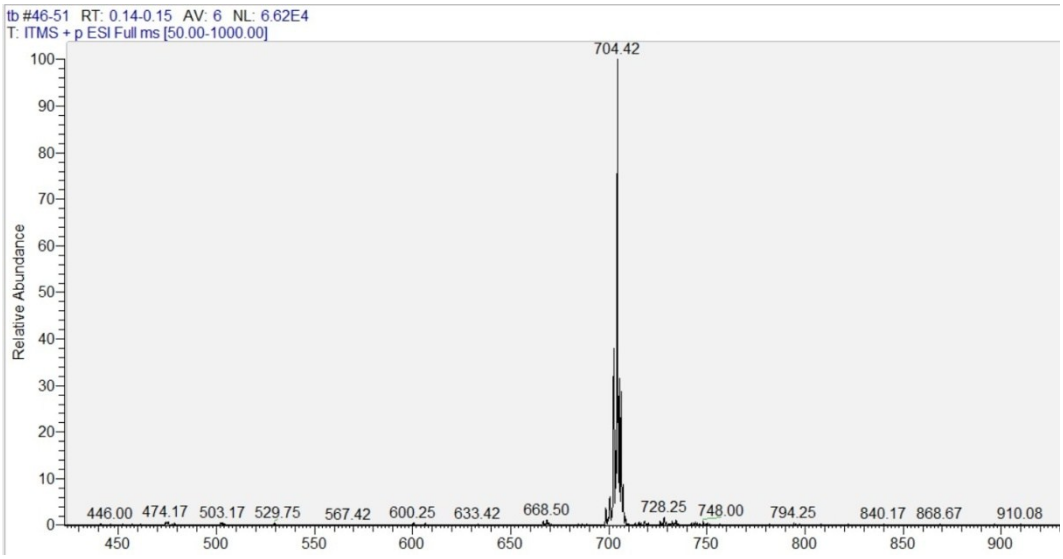

Fig. S3 Electrospray mass spectrometry (ES-MS) of **Ir-R** in CH_2Cl_2-CH_3OH solution.

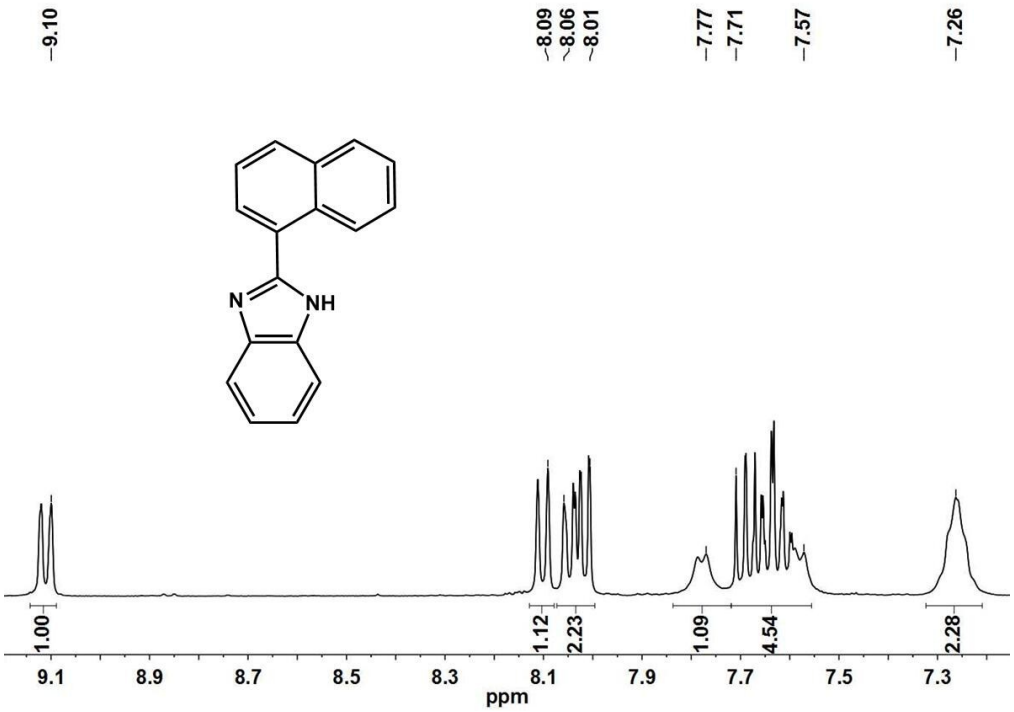

Fig. S4 ^{1}H NMR spectrum of nbiH (400 MHz, DMSO-d_6).

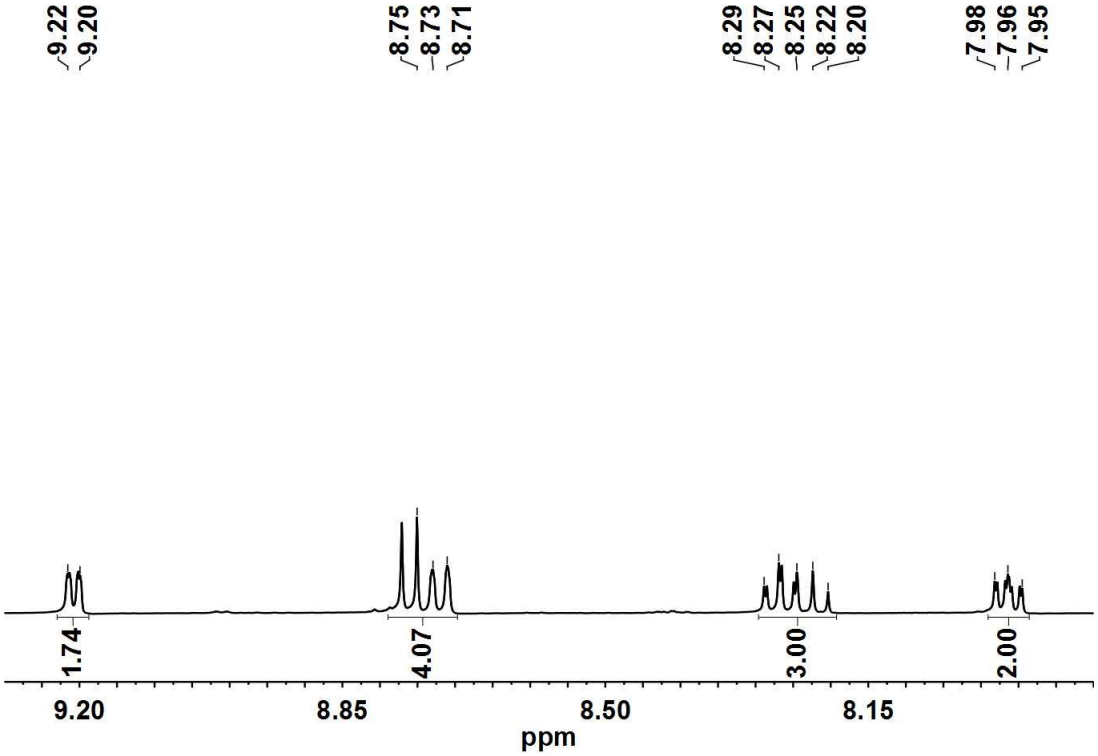

Fig. S5 ^{1}H NMR spectrum of Ir(tpy)Cl_3 (400 MHz, DMSO-d_6).

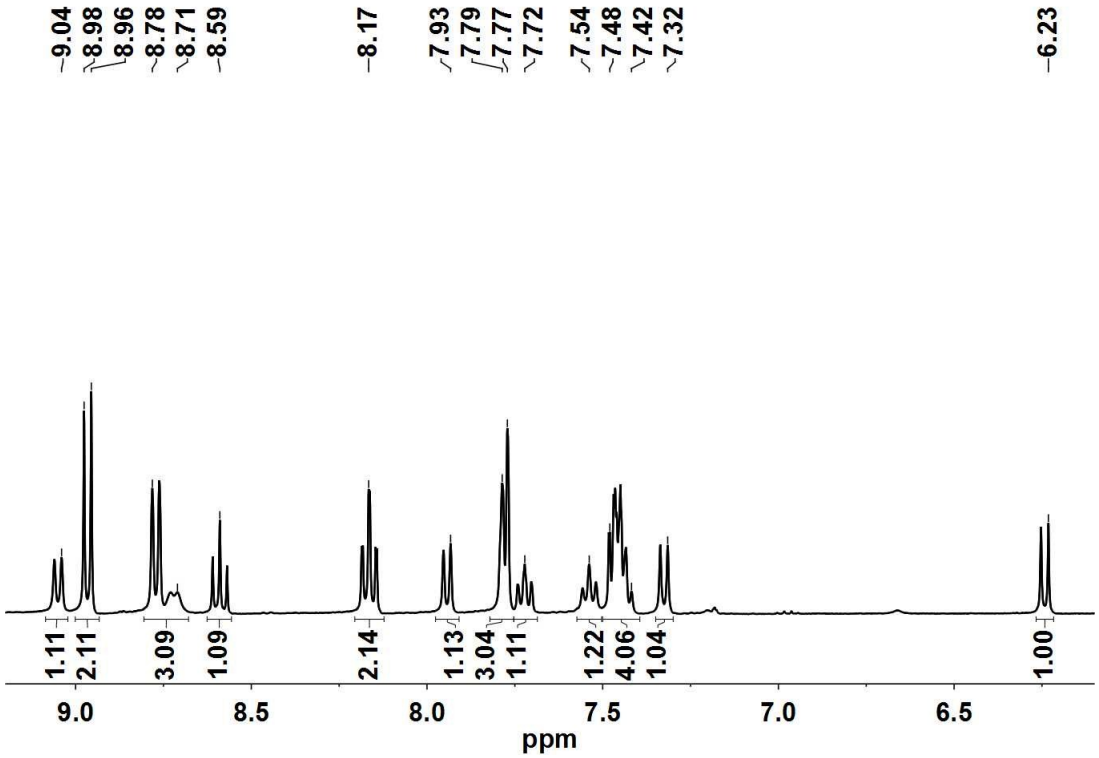

Fig. S6 ^{1}H NMR spectrum of **Ir-O** (400 MHz, DMSO-d_6).

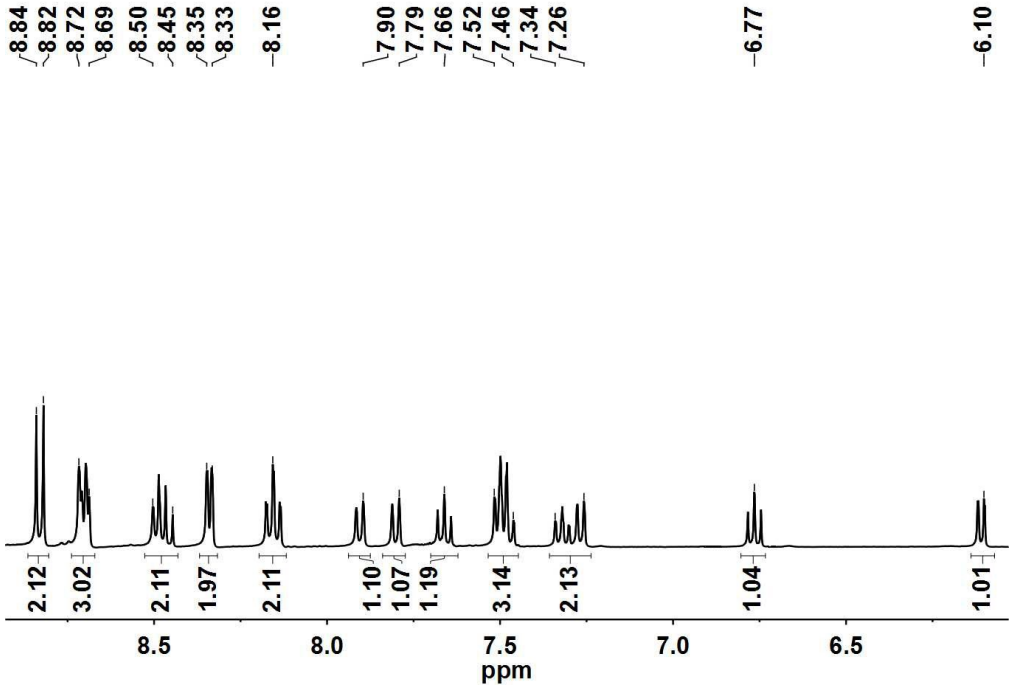

Fig. S7 ^{1}H NMR spectrum of **Ir-R** (400 MHz, DMSO-d_6).

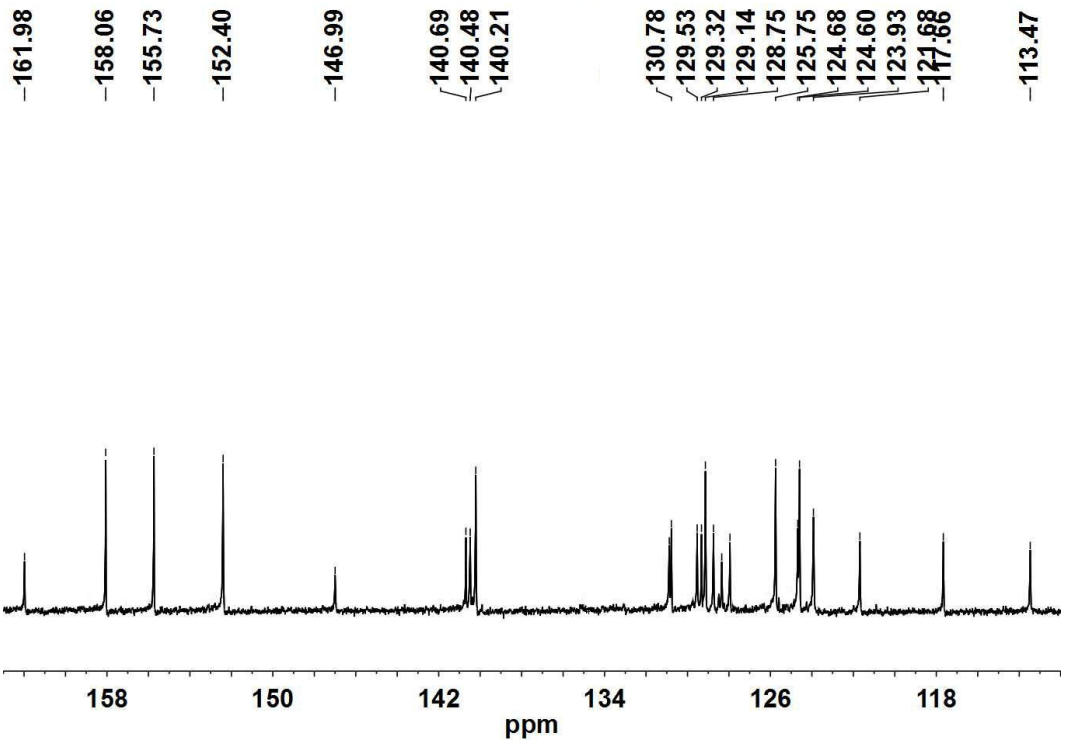

Fig. S8 ^{13}C NMR spectrum of **Ir-O** (500 MHz, DMSO-d_6).

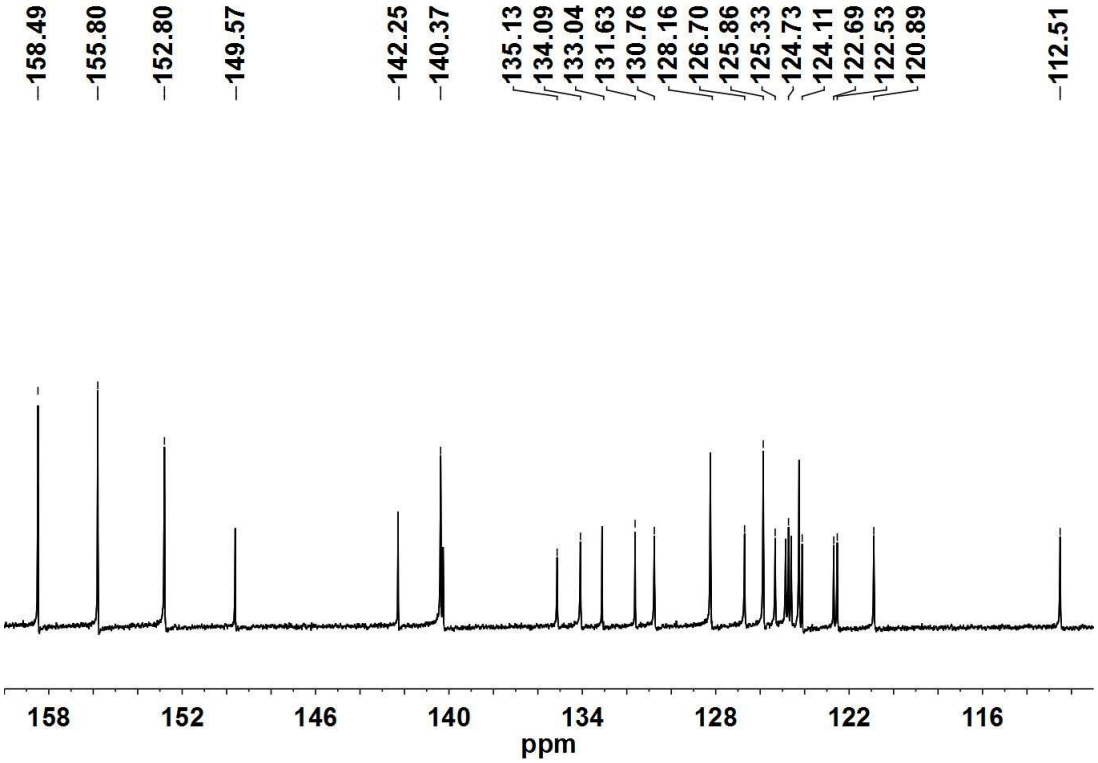

Fig. S9 ^{13}C NMR spectrum of **Ir-R** (500 MHz, DMSO-d_6).

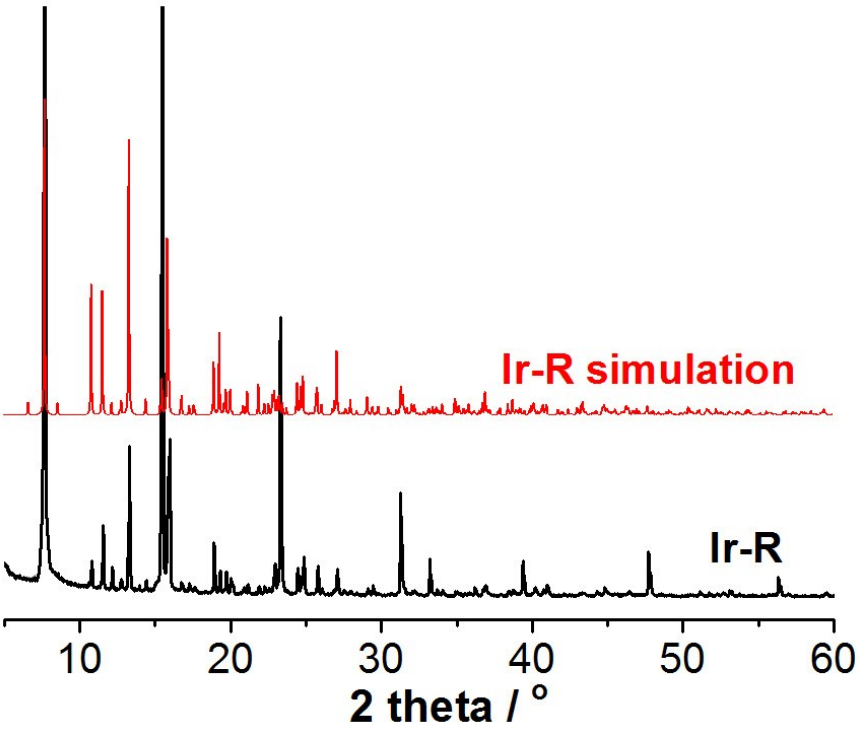

Fig. S10 Experimental and simulated XRD patterns of **Ir-R**.

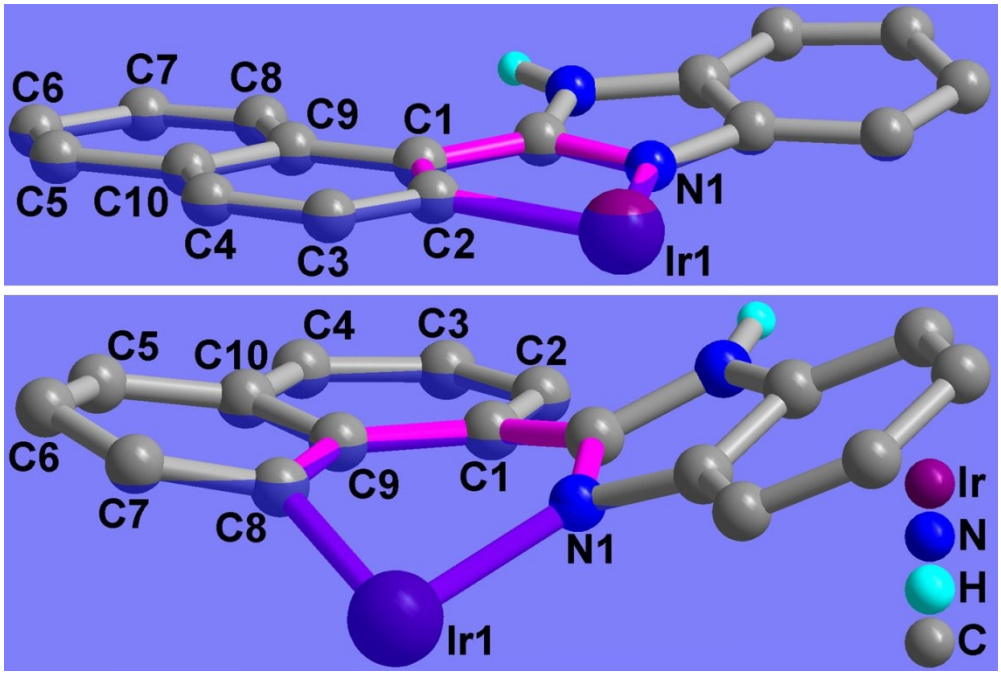

Fig. S11 The nbi$^-$ lignds in **Ir-O**·Et_2O·CH_3COCH_3 (top) and **Ir-R** (bottom) showing different twist extent and coordination mode.

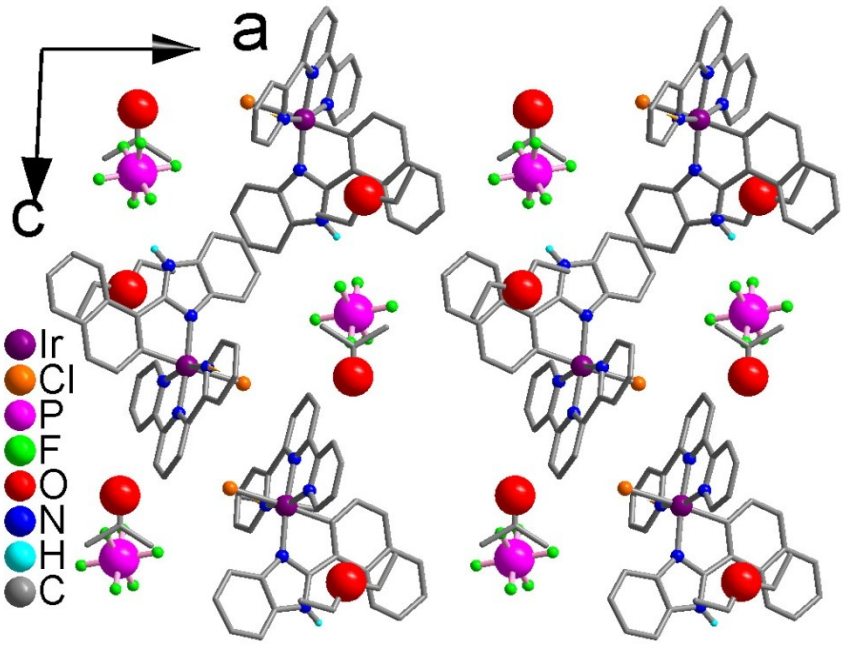

Fig. S12 The packing structure of **Ir-O**·Et_2O·CH_3COCH_3, in which supramolecular chains along *b* axis are held together by van der Waals interactions.

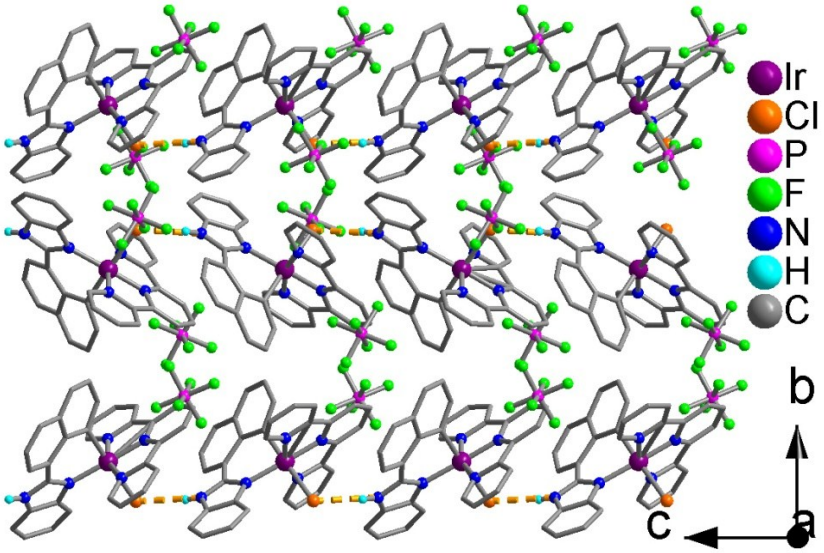

Fig. S13 The packing structure of **Ir-R** in which supramolecular chains along *c* axis are held together by van der Waals interactions.

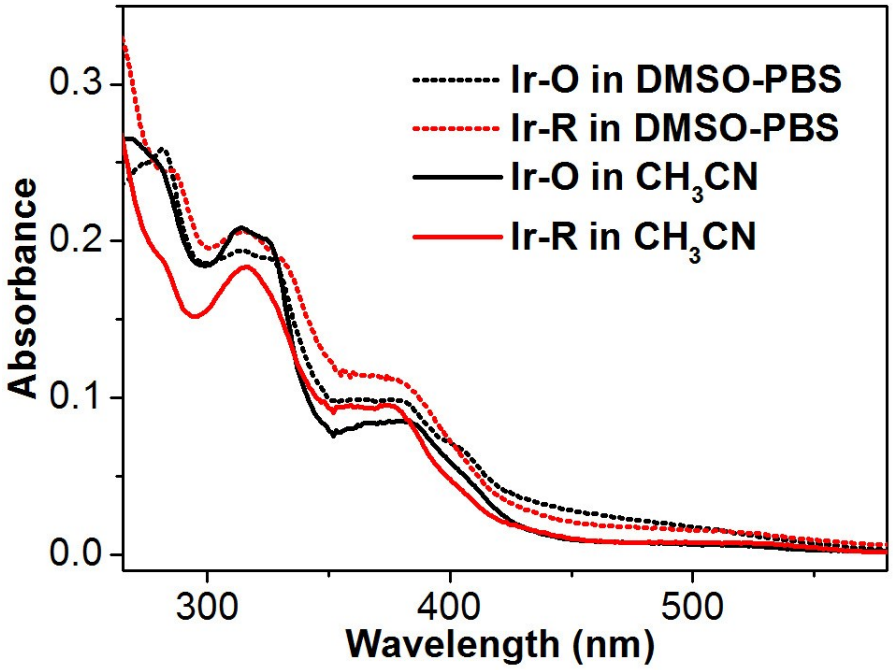

Fig. S14 UV-vis absorption spectra of **Ir-O**, **Ir-R** in CH_3CN and in phosphate buffer solution (PBS, pH = 7.4) containing 10% DMSO.

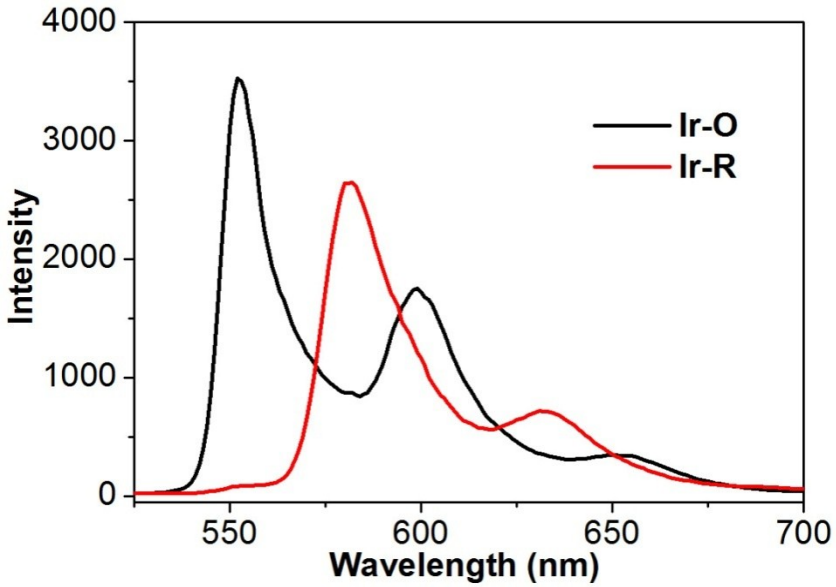

Fig. S15 Phosphorescence spectra of **Ir-O** and **Ir-R** in C_2H_5OH-CH_3OH (v/v = 3/1) at 77 K (c = 1.0 × 10^{-4} M, λ_{ex} = 398 nm).

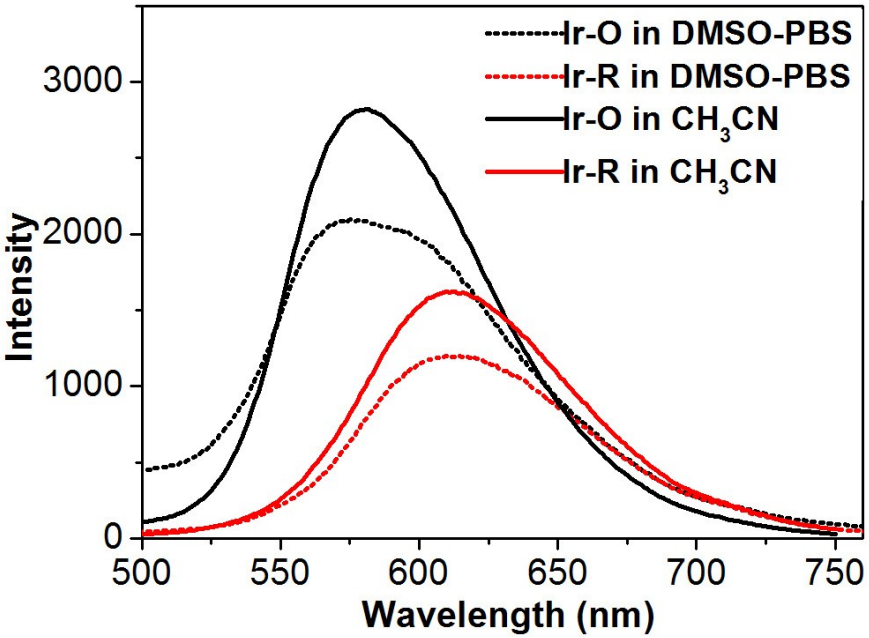

Fig. S16 The luminescence spectra of **Ir-O** and **Ir-R** in CH_3CN and in phosphate buffer solution (PBS, pH = 7.4) containing 10% DMSO (c = 1 × 10^{-4} M, λ_{ex} = 398 nm).

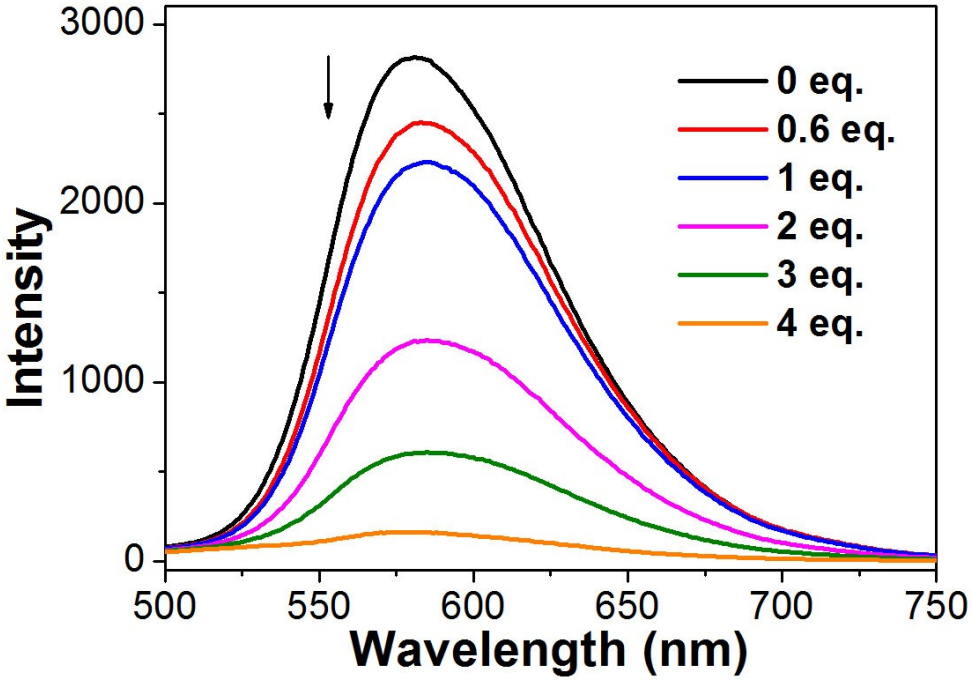

Fig. S17 Luminescence spectral changes of **Ir-O** in CH_3CN (c = 1 × 10^{-4} M, λ_{ex} = 398 nm) upon adding tetrabutylammonium hydroxide (TBAOH).

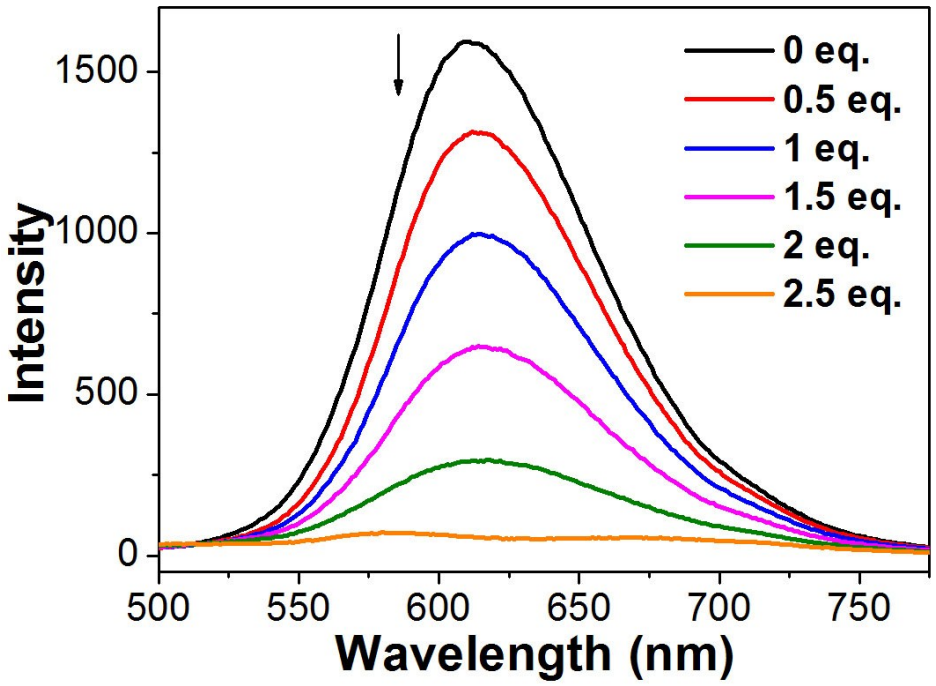

Fig. S18 Luminescence spectral changes of **Ir-R** in CH_3CN (c = 1 × 10^{-4} M, λ_{ex} = 398 nm) upon adding tetrabutylammonium hydroxide (TBAOH).

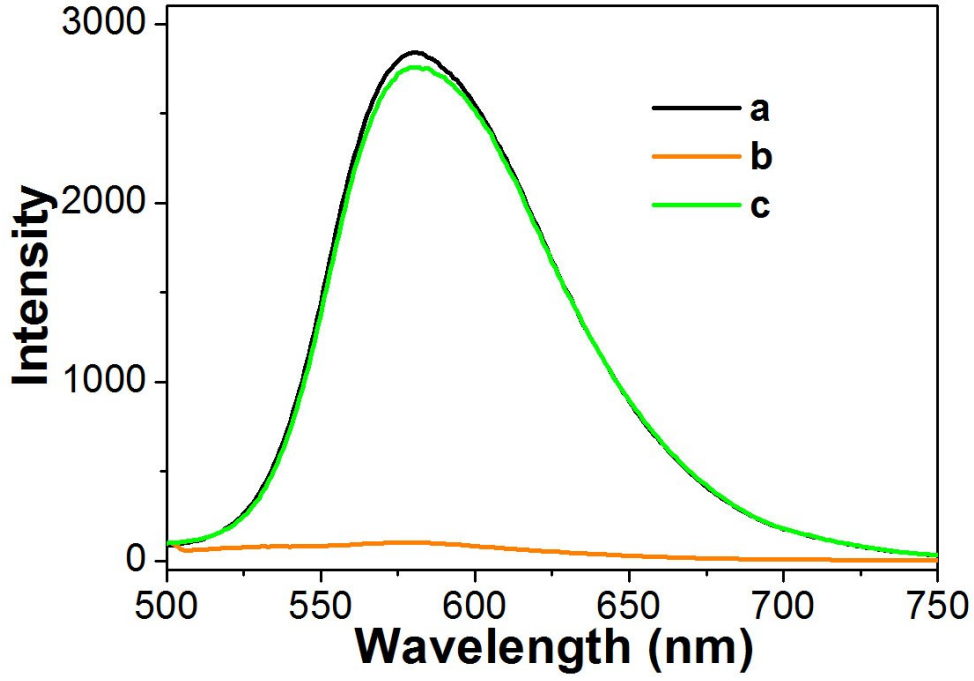

Fig. S19 Luminescence spectra of **Ir-O** (c = 1 × 10^{-4} M, λ_{ex} = 398 nm) in CH_3CN (plot a), in CH_3CN containing 4 eq. TBAOH (plot b), and in CH_3CN containing 2.5 eq. TBAOH and 4 eq. TFA (plot c).

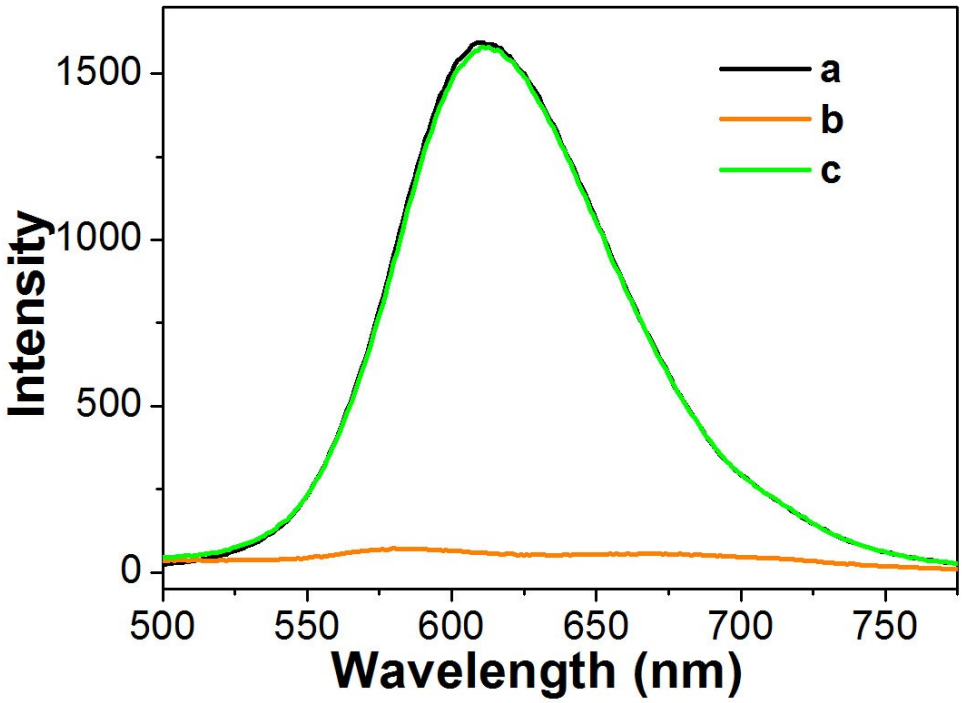

Fig. S20 Luminescence spectra of **Ir-O** (c = 1 × 10^{-4} M, λ_{ex} = 398 nm) in CH_3CN (plot a), in CH_3CN containing 2.5 eq. TBAOH (plot b), and in CH_3CN containing 2.5 eq. TBAOH and 2.5 eq. TFA (plot c).

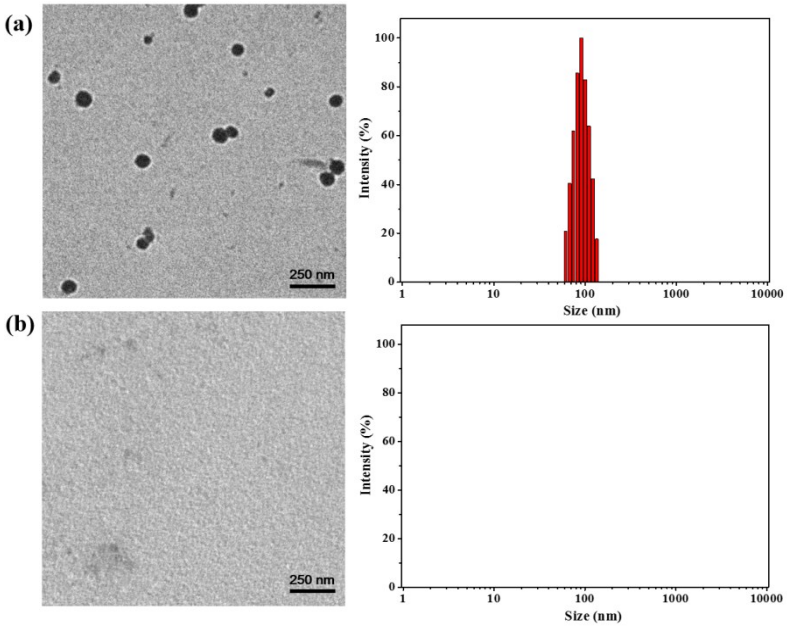

Fig. S21 TEM images (left) and size distributions measured by DLS (right) of **Ir-O** (a) and **Ir-R** (b) in H_2O (c = 20 μM).

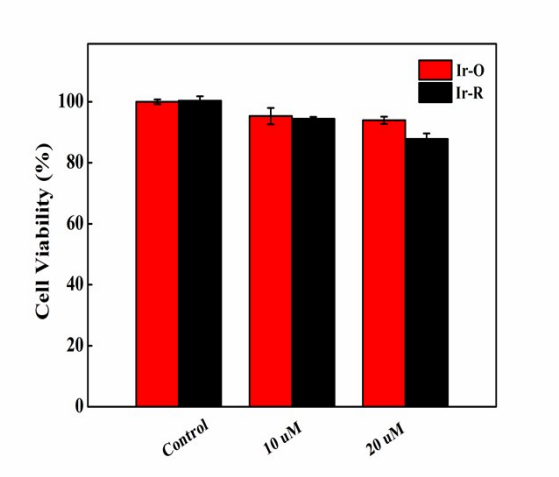

Fig. S22 The cell viability of HeLa cells incubated with different concentrations of **Ir-O** and **Ir-R** for 24 h. Data bars show mean ± s.d. (*n* =5 technical replicates).

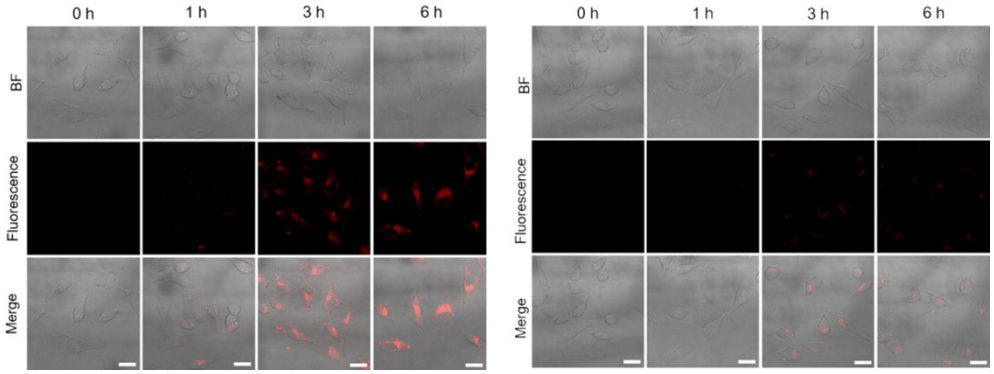

Fig. S23 Confocal laser scanning microscopy (CLSM) images of living Hela cells incubated with 20 ìM **Ir-O** (left, pseudo red color) or **Ir-R** (right, pseudo red color) at 37 °C for different time. Scale bar: 50 ìM.s

References

S1 J.-P. Collin, I. M. Dixon, J.-P. Sauvage, J. A. Gareth Williams, F. Barigelletti, L. Flamigni, *J. Am. Chem. Soc.*, 1999, **121**, 5009.

S2 D.-P. Gong, T.-B. Gao, D.-K. Cao and M. D. Ward, *Dalton Trans.*, 2017, **46**, 275.

S3 SAINT, Program for Data Extraction and Reduction, Siemens Analytical X-ray Instruments, Madison, WI, 1994–1996.

S4 (*a*) SHELXTL, Reference Manual, version 5.0, Siemens Indus-trial Automation, Analytical Instruments, Madison, WI, 1997; (*b*) G. M. Sheldrick, *Acta Crystallogr., Sect. A: Fundam. Crystallogr.*, 2008, **64**, 112.